Detailed Health Monitoring of Large-Scale Urban Infrastructure by Combining Optical and SAR Images

Yufang He, Lifeng Niu, Guangzong Zhang, Jiaye Li, Tong Liu, Jian Liu, and Bo Chen, *Member, IEEE*

***Abstract*—In recent years, due to the influence of surface activities caused by natural factors and human activities, numerous infrastructures in urban areas have safety issues involving slow and severe deformation, necessitating detailed health monitoring and hazard identification. Although the interferometry synthetic aperture radar (InSAR) technology can achieve high-precision in slow deformation monitoring, it is difficult to capture the deformation signals of infrastructure caused by external forces or violent self-generated deformation due to loss of coherence. Besides, urban ground object changes can readily lead to deformation of urban infrastructure, as manifested in the deformation maps monitored by InSAR technology. Therefore, this article proposes an innovative method for investigating detailed urban infrastructure health monitoring by combining InSAR technology and change detection based on multitemporal remote sensing data. The study area comprises Guangzhou and Foshan in China experiencing significant urbanization. First, small baseline subset InSAR and independent component analysis are used to explain the spatio-temporal patterns of urban infrastructure with slow deformation in Guangzhou and Foshan. Subsequently, the ChangeClip model is employed to automatically detect drastic change activities of the infrastructure based on multi-temporal imagery. It is found that not a few infrastructures suffered sharp deformation such as road compression, building demolition and construction, and others. Finally, by overlapping the surface change detection map and urban infrastructure deformation map, specific causes and detailed health monitoring of urban infrastructure are identified. It is found that there are not a few buildings and subways with obvious slow and severe deformation behavior. Some infrastructures still have obvious deformation behavior in Guangzhou and Foshan, which requires further monitoring. All in all, by combining optical change detection and InSAR techniques, we could not only monitor slow and severe deformation for large-scale urban infrastructure, but also identify the deformation trigger factors and detailed hazards, and thus, provide valuable information for future urban development.**

***Index Terms*—Change detection, large-scale urban infrastructure, small baseline subset interferometry synthetic aperture radar (SBAS-InSAR), slow and severe deformation.**

I. Introduction

THE rapid progress of urbanization and the intense economic activities of humans have led to the deformation of numerous urban infrastructures across the globe. It poses significant threats to human life safety and leads to substantial economic losses [1], [2], [3], [4]. These facts have impelled us to sustain and expand the systematic deformation monitoring of large-scale urban infrastructure. Interferometry synthetic aperture radar (InSAR) technology has the advantages of wide coverage, high precision and being capable of all-weather monitoring, which gradually has matured and been widely used to measure urban infrastructure deformation [5], [6], [7], [8]. Urban activities such as construction and groundwater extraction lead to severe infrastructure deformation.

Recently, there are numerous studies on the slow deformation monitoring and causes analysis of large-scale urban infrastructure urban infrastructure based on InSAR technology. The persistent scatterer (PS) and small baseline subset (SBAS) InSAR methods, are particularly applied for monitoring differential displacements of urban infrastructure such as buildings and metro subways [4], [9]. Several studies have focused on the application of PS motion rates for monitoring displacements of individual urban infrastructure [10], [11], [12]. At the same time, more detailed deformation characteristics of buildings were monitored through the utilization of very high-resolution spotlight data [11], [12]. Multisource data like global positioning system, traditional leveling, land-use, and many techniques like geographic information system, light detection and ranging (LiDAR), are combined to improve deformation monitoring and make risk analysis for urban buildings and subways based on InSAR technology [4], [13], [14], [15], [16]. Besides, deep learning like the region-based convolutional neural networks and static analysis like fast independent component analysis

Received 20 January 2025; revised 29 March 2025 and 6 June 2025; accepted 15 July 2025. Date of publication 23 July 2025; date of current version 3 September 2025. This work was supported in part by the National Key Research and Development Program of China under Grant 2022YFF0503900, in part by the Natural Science Foundation of Guangdong Province under Grant 2022A1515010113, and in part by the Natural Science Foundation of Shenzhen under Grant GXWD20220811163556001. *(Corresponding author: Bo Chen.)*

Yufang He is with the School of Environment and Civil Engineering, Dongguan University of Technology, Dongguan 523820, China, also with the School of Aerospace, Harbin Institute of Technology (Shenzhen), Shenzhen 150001, China, and also with the Guangdong Provincial Key Laboratory of Intelligent Disaster Prevention and Emergency Technologies for Urban Lifeline Engineering, Dongguan University of Technology, Dongguan 523820, China (e-mail: heyufang0823@163.com).

Lifeng Niu, Guangzong Zhang, and Jian Liu are with the School of Aerospace, Harbin Institute of Technology (Shenzhen), Shenzhen 150001, China (e-mail: 20b958034@stu.hit.edu.cn).

Jiaye Li is with the School of Environment and Civil Engineering, Dongguan University of Technology, Dongguan 523820, China (e-mail: lijiaye@dgut.edu.cn).

Tong Liu is with the Department of Land Surveying and Geo-Informatics, The Hong Kong Polytechnic University, Hong Kong, SAR, China (e-mail: tong2.liu@polyu.edu.hk).

Bo Chen is with the School of Aerospace, Harbin Institute of Technology (Shenzhen), Shenzhen 518000, China, and also with the Key Laboratory of Aerospace Remote Sensing Big Data Intelligent Processing and Application of Guang-dong Higher Education Institutes, Shenzhen 518000, China (e-mail: hitchenbo@hit.edu.cn).

Digital Object Identifier 10.1109/JSTARS.2025.3592033

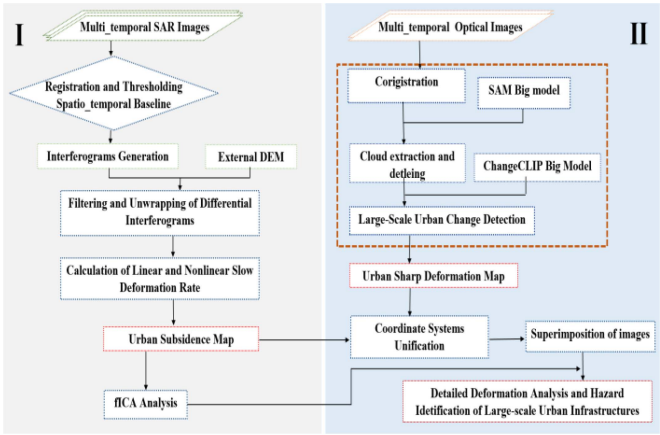

Fig. 1. Workflow of the method.

(FastICA) methods are developed to assess the ground deformation characteristic and make the deformation causes analysis [17], [18], [19].

Although the InSAR technology demonstrates proficiency in high-precision monitoring of slow deformation, it encounters difficulties in capturing the deformation signals of infrastructure when coherence loss occurs due to severe deformation. Some studies have been presented for the monitoring of sharp deformation for urban infrastructure [20], [21]. Besides, there are relatively few studies on automatical causes analysis and detailed hazards of urban subsidence at present [22]. Thus, we put forward a proposal to combine InSAR and optical remote sensing technologies, aiming at the meticulous health monitoring of urban infrastructure, such as building groups and subway lines. It can also unravel deformation causes and identify detailed hazards of large-scale urban infrastructure.

The core concept of this article is to apply optical and SAR images to further improve the health monitoring of urban infrastructure in detail. We propose a new method by integrating sharp deformation like land cover changes obtained from optical images with slow deformation results derived from SAR images. The methodology is presented next, and the research area along with the datasets is introduced. Finally, we combine slow and sharp urban deformation data to analyze their causes. Detailed hazard identification is then performed by overlaying urban surface changes with subsidence results.

II. Methodology

In this article, SBAS-InSAR and change detection techniques for monitoring slow and severe deformation of urban infrastructure were applied. Fig. 1 shows the detailed workflow. First, an urban subsidence map is produced by using the SBAS-InSAR technique based on multitemporal SAR images and a DEM, provided by the shuttle radar topography mission. The SAR time series images are co-registered, and FastICA method is applied to obtain the deformation spatio-temporal patterns [18], [19].

Then a highly precise urban surface change map is obtained based on multitemporal optical Google Earth imagery. The cloud detection and change detection were operated by using segment anything model (SAM) and ChangeClip big model to obtain the urban ground object sharp change map [23], [24], [25]. Finally, by overlaying the surface change map with the urban deformation map of infrastructures, the deformation-triggering factors and specific hazards can be obtained.

A. Time Series Slow Deformation Inversion and ICA Decomposition Method

SBAS-InSAR technique has been proposed by Berardino, who provided a detailed introduction to its principle, data processing order, and multiple application cases [26]. All differential interferograms are generated based on the subset conditions of automatically combined SAR interferograms. However, it is not typical for all differential interferograms to exclusively belong to a single subset, which results in a singular matrix that generates an infinite array of potential solutions. In this case, the singular value decomposition and iterative reweighted least squares method are applied to acquire the pseudoinverse B of the matrix and thereby obtain its minimum normal solution [9]. Subsequently, the topographic residual phase and the deformation phase are estimated. However, the time series phase might introduce significant discontinuities like atmospheric delay, leading to physically meaningless results. Thus, the generic atmospheric correction online service for InSAR interferometric correction and a polynomial fitting model were employed to effectively eliminate atmospheric errors [27].

To obtain the spatio-temporal deformation patterns, the independent component analysis (ICA) method is applied. It can discern and isolate physical deformation signals stemming from diverse factors, including geological activities, construction activities, and environmental alteration. As an advanced statistical approach tailored for processing and analyzing multidimensional random vector data. It transforms intricate multidimensional datasets into components that exhibit maximal independence, facilitating dimensionality reduction and feature extraction to identify and separate the principal independent factors present in the data [28]. In particular, the FastICA algorithm is leveraged, efficiently decomposing the mixed signal matrix X into a set of ns statistically independent sources over time [19]. Initially, the ground deformation time series is modeled as follows:

$$X \cdot (t \cdot p) = A(t \cdot n) \cdot S(n \cdot p) \tag{1}$$

where A is a mixed matrix, S is the independent component (IC) matrix, n is the number of ICs considered, and p, t represents the number of pixels and the number of dates, respectively. Fixed-point iteration is used to derive the convergent solutions of the mixing matrix A and the source matrix S by maximizing the spatial non-Gaussianity of the sources.

B. Detailed Deformation Analysis and Hazard Identification of Large-Scale Urban Infrastructure

To detect the sharp deformation like urban cover type changes with higher accuracy, high-resolution Google Earth images were used. Clouds and their shadows are present in most optical images, which can obscure or distort the true ground features.

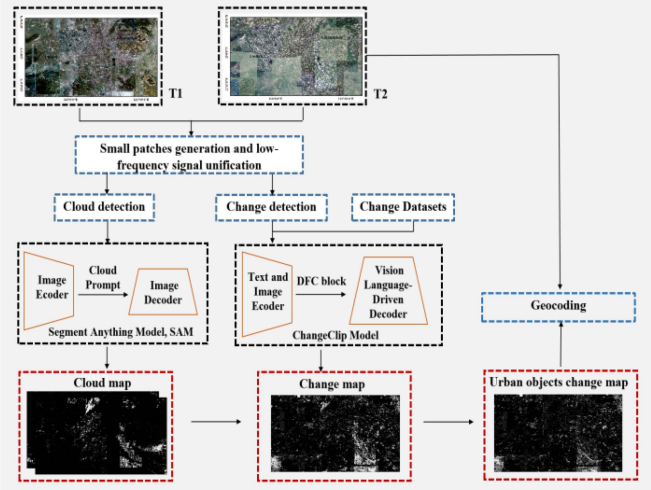

Fig. 2. Detailed workflow for cloud extraction and change detection of multitemporal optical images.

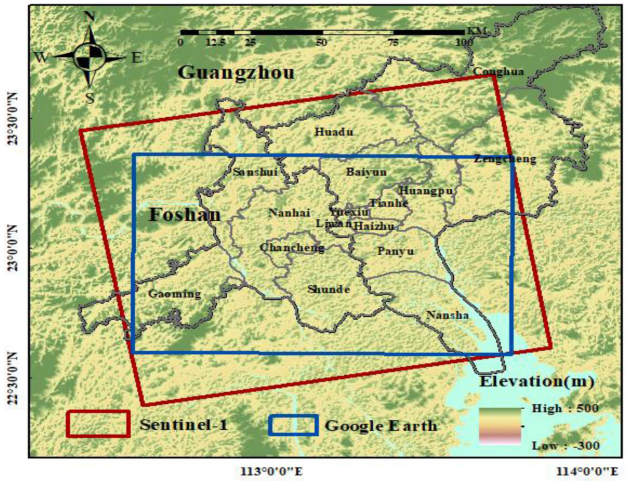

Fig. 3. Location of the research area. The red and blue frames embrace the locations of the Sentinel-1 and Google Earth images used in the study.

Fig. 2 shows the detailed workflow for cloud extraction and change detection based on the two temporal optical images. Identifying clouds and removing them from images is very critical. Moreover, the intricate shape and texture of clouds pose a challenge for detection algorithms that rely on rudimentary shape and texture features in analyzing RGB images. In this context, SAM big model has become the most promising method for the pre-processing of RGB real color satellite imagery [23].

First, we divide the optical RGB images into patches with the size of 256 × 256. Then, we incorporate cloud-related text prompts and point prompts, which are processed through the cloud prompt mechanism based on the Image Encoder and Image Decoder. Finally, we utilize the SAM to remove cloud-affected pixels, resulting in a cloud distribution map of the optical remote sensing images. The network structure employs skip connections to facilitate image segmentation, which effectively extracts the cloud pixels from the image with zero-shot.

Considering the specific urban change types of the area, we applied the ChangeClip model. It offers a more precise depiction of the condition of urban surface objects, such as construction activities [25]. Before the operation of change detection, the Fast Fourier Transform is used to unify the low-frequency components of T1 and T2 optical RGB patches. By doing so, it usually highlights the difference between the changed areas and suppresses the unchanged areas. Next, we set up the environment for the ChangeClip model, the relevant parameters, and then incorporate change detection prompts. By applying the ChangeClip model, we perform change detection and generate a change detection map. Finally, the cloud map obtained before was used to delete the clouds distorting from the change map.

To obtain the detailed deformation monitoring and hazard identification of urban infrastructure, it is crucial to unify the coordinates of the urban surface change detection map and the InSAR-based deformation map. Then the feature matching method was applied to co-register them. Then we carried out an in-depth deformation analysis of the urban infrastructure, which includes slow deformation and sharp change. Building contours and subway lines are used for detailed analysis of urban infrastructure deformation. Then a detailed hazard identification of urban infrastructure is carried out by removing the urban surface change patches from the urban deformation map.

III. Research Area and Images Datasets

Guangzhou and Foshan are located in the south-central region of Guangdong Province, China, which are built on a complex geological environment with a widespread distribution of silty soft soils. The climate features sweltering heat and humidity during the summer months, while the winter season brings cooler and drier conditions. The study area receives an annual rainfall of approximately 1700 mm, with the rainy season lasting from April to September. The high annual rainfall in these regions may further contribute to ground subsidence. Fig. 3 displays the location of the research area of Guangzhou and Foshan. In February 2018, a road collapse occurred on the east-west side of the Jihua West Road First Ring Bridge in Foshan, resulting in the tragic loss of 11 lives and an economic loss of 53.238 million RMB [30]. As a result, it has become imperative to conduct a comprehensive analysis of land subsidence and assess the potential hazards associated with it.

For the experiment, 110 C-band Sentinel-1 SAR images with an ascending orbit were acquired from the study area between March 12, 2017 and December 21, 2020. The spatial resolution of Sentinel-1 SAR images is about 15 m. Fig. 3 displays the extent of the SAR datasets used in the study, covering Foshan and Guangzhou. To generate the urban surface change map for sharp deformation, we used Google Earth optical imagery. The two images with the spatial resolution of up to 2.5 m were captured on January 1st, 2017 and January 1st, 2021, respectively. The specific parameters of SAR and optical images are given in Table I. Through a comparative analysis of the two sets of images, we pinpointed regions experiencing substantial alterations, enabling us to monitor the evolution of land use patterns. This analysis proved vital for our investigation into urban infrastructure deformation.

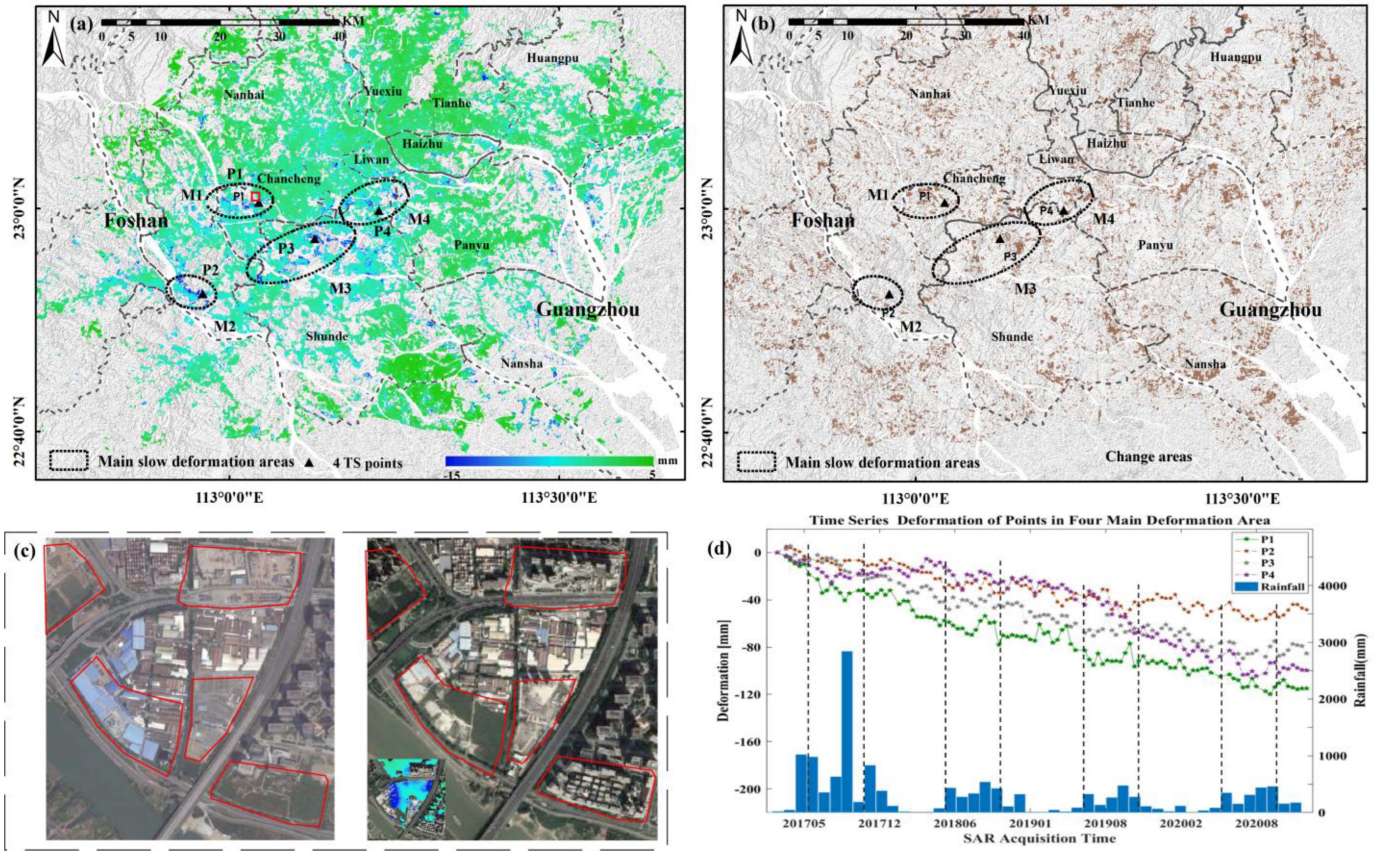

Fig. 4. (a) Annual average deformation of the LoS direction for impervious surface from March 2017 to April 2020. (b) Urban surface change the whole research area from March 2017 to April 2020. (c) Ground surface changes in the red-boxed area of M1. (d) Cumulative deformation in the LoS direction curves over time of InSAR-driven scatterers are calculated from the four main subsidence areas M1(b), M2(c), M3(d), M4(e). Blue and brown colors show slow deformation in the LoS direction and sharp deformation, respectively.

TABLE I
SPECIFIC PARAMETERS OF SAR AND OPTICAL IMAGES

Parameters	Optical imagery	SAR imagery
Satellite	QuickBird, Landsat-7	Sentinel-1
Acquisition dates	20170101/20210101	20170312/20201221
The spatial resolution	2.5m	15m

IV. RESULTS AND DISCUSSION

In this experiment, the urban annual deformation rate of Guangzhou and Foshan was calculated using the SBAS-InSAR technology based on 110 Sentinel-1A images with ascending orbits. The two key parameters of the time baseline and the spatial baseline are set to 90 days and 150 m respectively. The displacements were detected in the line of sight (LoS) direction. Fig. 4 shows the annual slow and sharp deformation of impervious surfaces within the research area from March 2017 to April 2020. In Fig. 4(a), four large-scale land subsidence funnels of varying sizes can be observed in the northwest of Chancheng District, the south of Nanhai District, and the north and southeast of Shunde District (labeled as M1 to M4) in two cities. Besides the prominent large-scale subsidence regions in M1 to M4, numerous small- scale subsidence funnels are also identified in these areas. This significantly differs from the large-scale subsidence phenomena witnessed in other major cities like Xi'an, China. In such cities, a large portion of the large spatial scale (tens of kilometers) subsidence is mainly due to excessive groundwater extraction [1]. It is found that there are severe deformation areas detected in M1 to M4 of Fig. 4(b).

Fig. 4(c) offers the significant surface changes of the region enclosed by the red box in subsidence area M1. The irregular red polygons demarcate the ground surface changes as observed from two temporal optical images acquired between January 2017 and January 2021. Notably, these regions of gradual deformation detected by InSAR technology are consistently encompassed by areas undergoing substantial surface changes. It clearly reveals a strong correlation between these two types of deformation. Four InSAR coherence scatterers were selected from the four principal subsidence areas (M1–M4), and their cumulative deformation curves over time are illustrated in Fig. 4(d), which also shows the monthly rainfall variations during the same period. These curves primarily display linear changes with slight periodic oscillations.

To further explore the spatiotemporal characteristics of deformations, we further used the FastICA algorithm. First, the principal component analysis (PCA) algorithm was utilized to perform noise reduction on the time series of cumulative

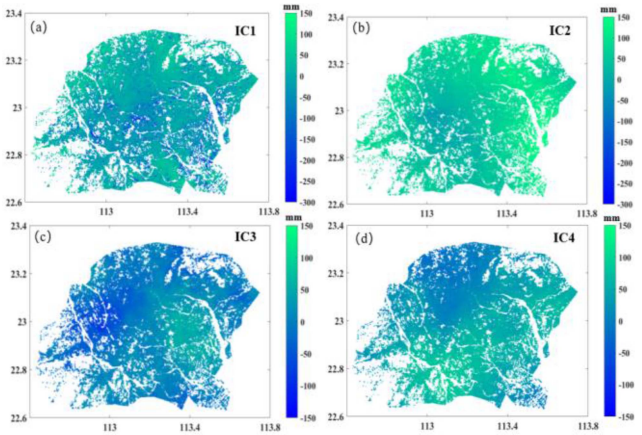

Fig. 5. Four different spatial deformation patterns, IC1 to IC4 (a, b, c, d) obtained by the FastICA. The *X*-axis represents the geographic longitude, and the Y-axis represents the geographic latitude.

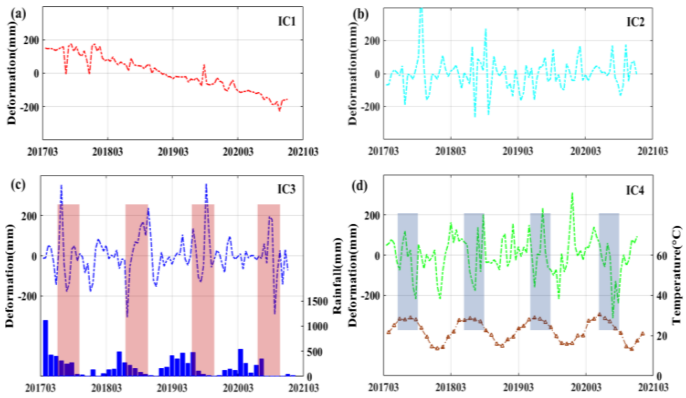

Fig. 6. Four different temporal deformation patterns, IC1 to IC4 (a)–(d), obtained by the FastICA. The four spatial deformation patterns depict the evolution of temporal deformations from March 2017 to December 21, 2020. The right vertical axes in panels (c) and (d) represent the monthly variations in precipitation and mean temperature, respectively, during the corresponding observation period.

deformation. The standardization of the deformation matrix and the variance noise reduction method were both applied to enhance the stability of ICA solutions, while the whitening process was turned OFF. After assuming the existence of four independent temporal deformation modes, we carried out the FastICA analysis. The results revealed that the characteristic values of the first four components together can explain about 71% (49%, 11.4%, 5.8%, 5.1%) of the cumulative signal variance.

We applied the FastICA algorithm to decompose the mixed signal matrix with dimensions of 159 780 × 110 (where 159 780 represents the number of selected coherent pixels, and 110 represents the number of selected SAR images) and convert it into a set of four statistically ICs (see Fig. 5) and a mixing matrix (see Fig. 6). Fig. 5 displays the first four distinct IC temporal deformation patterns, with the colorimetric scale representing the spatial distribution of cumulative deformation magnitudes. The time-series deformation is shown in Fig. 6. Four different spatial deformation patterns IC1 to IC4 from March 2017 to December 2020 are shown in Fig. 6, in which the horizontal coordinates represent time series, and the vertical coordinates represent deformation along the LoS directions. Fig. 6(e) and (f) represent the monthly variations in rainfall and average temperature, respectively, over the same period.

The spatial distribution of the deformation area of the IC1 component in Fig. 5(a) is dispersed throughout the study area, which is basically consistent with the above deformation distribution characteristics of the study area. The significantly high time dependent linear deformation of the IC1 is shown in Fig. 6(a), indicating the time series deformation pattern. There are also certain seasonal waves every summer, which may be related to an increased extraction of groundwater or rainfall. Based on our observations, we assume that the IC1 may be associated with the compaction of land cover objects in the vicinity, as well as local groundwater extraction and other factors. However, further research is needed to confirm this hypothesis. In contrast, the time characteristic vectors of IC2 [see Fig. 5(b)] displayed in Fig. 6(b) appear to be random, with oscillations that frequently cross the zero line. We postulate that this component may be linked to error signals.

As clearly shown in the pink boxes of Fig. 6(c), IC3 exhibits pronounced seasonal uplift and subsidence variations, which align with the seasonal patterns observed in rainfall data [see Fig. 5(c)]. It can be concluded that there is a seasonal atmospheric influence in the research area with a period of about one year. Fig. 6(d) shows the deformation feature time series of IC4 [see Fig. 5(d)] and temperature, using black and purple boxes to highlight those of IC4 and temperature variations. It has the characteristics of increased subsidence in summer and increased uplift in winter. As clearly demonstrated, IC4 exhibits sharp uplift and subsidence variations that closely follow the temperature curves, indicating a strong relationship between IC4 and seasonal changes in temperature. Therefore, IC4 may be related to temperature or rainfall in the research area. Preliminary analysis suggests that the deformation distribution of IC1 demonstrates substantial spatial correspondence (∼50% overlap) with the composite deformation patterns of Foshan and Guangzhou.

According to the detailed investigation, these subsidence areas are mainly affected by sharp land changes such as many construction activities, groundwater extraction and natural soil subsidence. We also found that there are many urban surface changes in areas M1 to M4 during the InSAR monitoring period based on the time series of imagery with high resolution. These urban surface change activities, which include the construction of new buildings, the expansion of suburban areas, preliminary ground works, and road expansions, are one of the main causes of the urban surface deformation. Such deformation would increase the difficulty of identifying detailed subsidence hazards.

A. Deformation Health Monitoring of Large-Scale Urban Building Blocks

In the monitoring of large-scale building deformations, both sharp and slow changes can be detected simultaneously by optical monitoring and InSAR technology, or by either one of

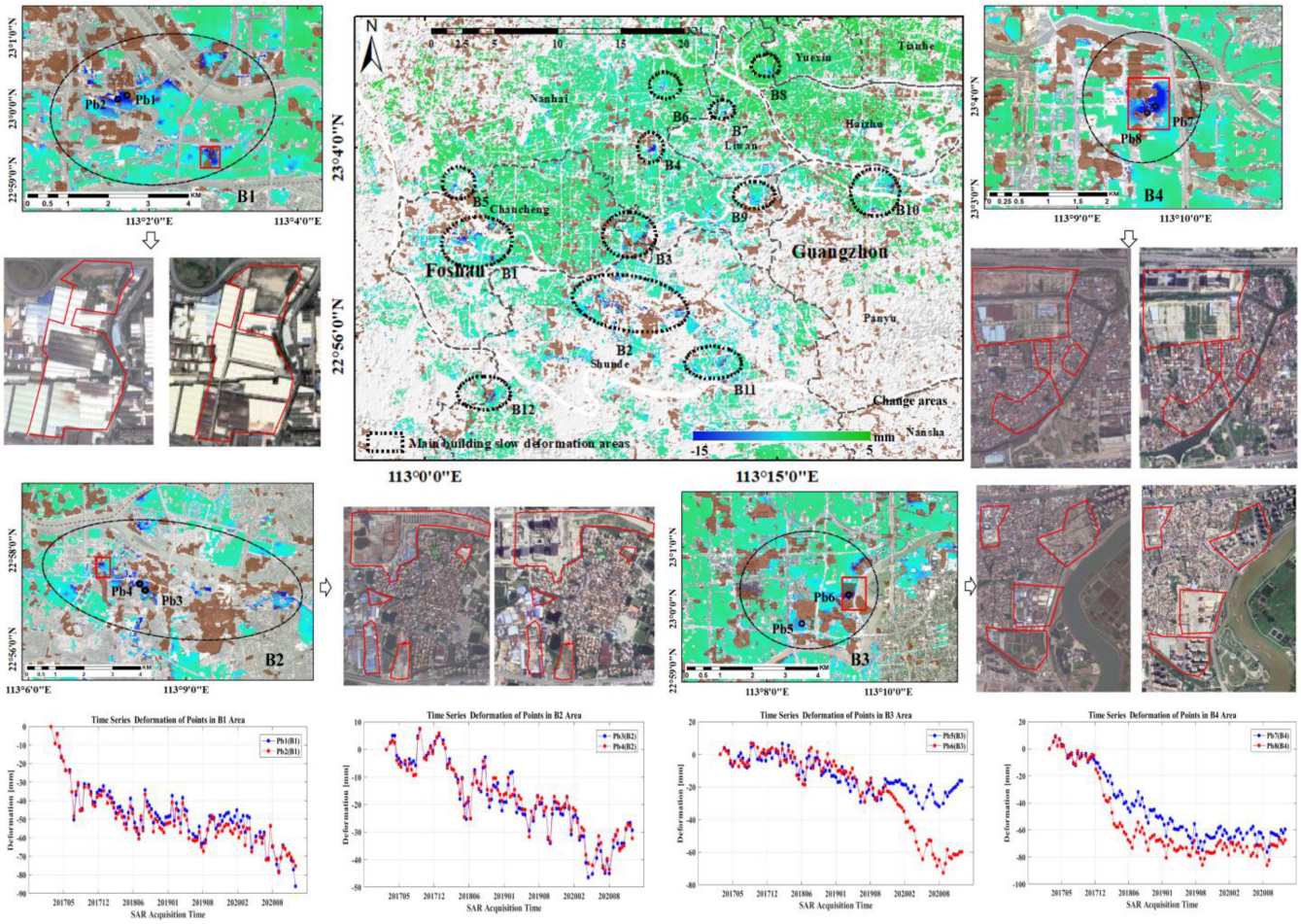

Fig. 7. Annual average subsidence along the LoS direction and urban surface change for building patches of the whole research area, four enlarged main subsidence areas (B1, B2, B3, and B4) from March 2017 to April 2020, and the cumulative deformation in the LoS direction curves over time of InSAR-driven CSc from the four main subsidence areas.

these techniques. Based on this, we conduct analyses of the causes of building deformations and detection of their actual hazards. Given the limited spatial resolution of sentinel-1 SAR data and the substantial geometric deformation and imaging discrepancies observed in individual building InSAR-driven scatterers, we performed block analysis on the building infrastructure to ensure its precise determination. Fig. 7 shows the building deformation and surface changes of building patches in Guangzhou and Foshan from early 2017 to late 2020. It is found that some building blocks exhibit significant ground subsidence values (B1–B12). In addition, many urban surface changes are identifiable such as suburban expansion and urban construction change based on RGB Google Earth imagery.

In particular, the deformation of buildings in the B1–B4 areas is relatively obvious, with some exceeding −10 mm. To more accurately pinpoint the genuine hazard of ground subsidence affecting urban buildings, we initially identified and extracted pixels of deformed buildings with the subsidence rate exceeding 5 mm per year, while also excluding blocks impacted by surface changes. The outcomes of this process are depicted in Fig. 7. Following the elimination of false hazardous areas resulting from surface changes, we observed that several buildings within the main urban zone of Guang and Foshan urban zone still exhibit high settlement rates. These are predominantly located in areas B1, B2, and B4.

Fig. 7 also shows the deformation rates in the LoS direction and obvious surface changes of the building clusters near Huyongyong Village (B1), Foshan Park (B2), Guangzhou Poly Garden (B3), and Foshan Shiwan Town (B4), respectively. It is found that buildings with significant deformations near the Lake Chung Chung (B1) and the Foshan Park (B2) exhibited fewer ground surface changes, whereas buildings with significant deformations near Baoli Garden (B3) and Shiwan Town (B4) in Foshan showed obvious ground surface changes based on two temporal optical images. This also indicates that the deformation of building clusters is not solely influenced by urban construction activities, but also associated with other factors that cannot be detected through optical imaging.

In Fig. 7, numerous buildings with significant subsidence magnitudes are observed, particularly in Huyongyong Village (B1), Wuzhuang Village (B5), Chancheng District, Foshan City, Xiaoyong Village (B2), Huadun Village (B11), and Yingming Village (B12). This is also true for buildings in Huyongyong Village (B1), Wuzhuang Village (B5) in Chancheng District,

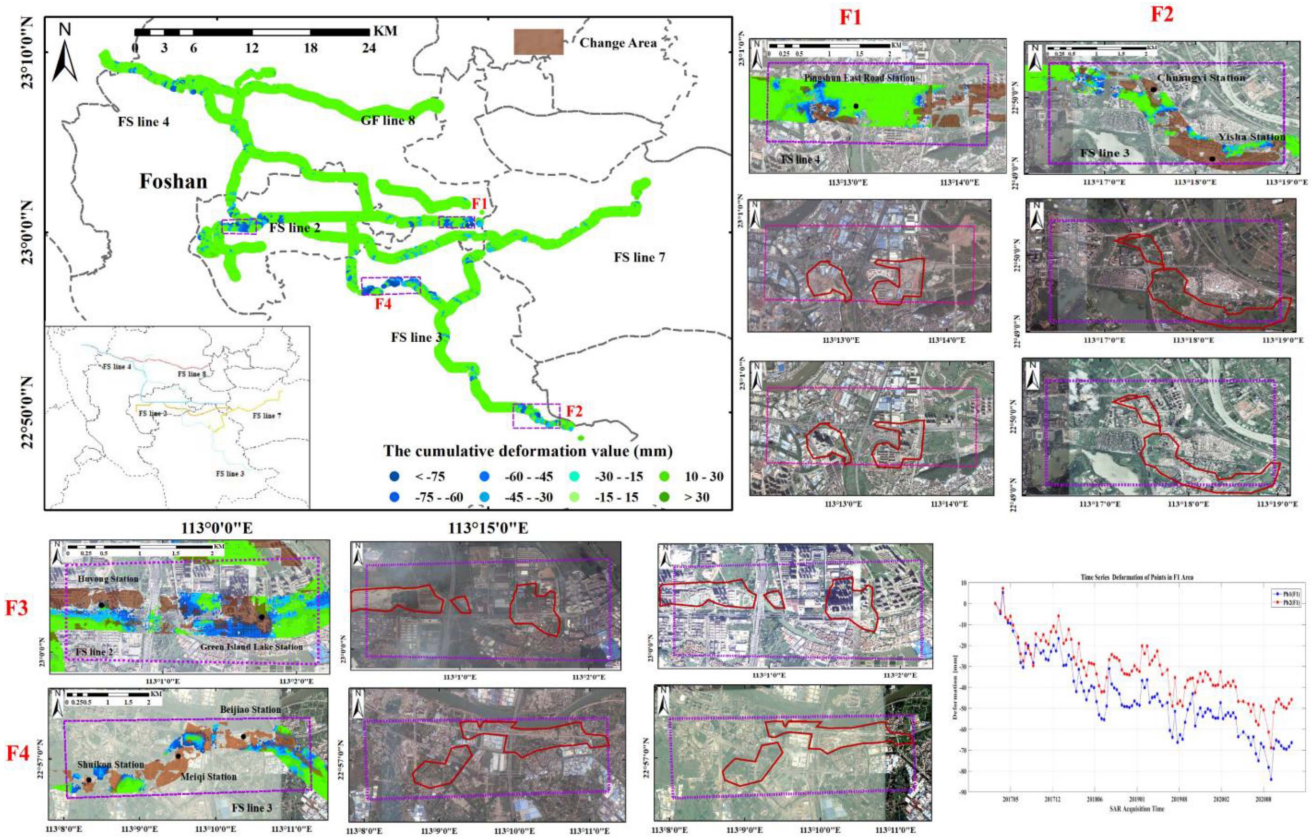

Fig. 8. Cumulative deformation along the LoS direction and urban surface changes for the subway line in Foshan from March 2017 to April 2020, four enlarged main subsidence areas of Foshan subway lines, namely F1, F2, and F3, and the curves of the cumulative deformation over time of InSAR—driven CSs from the main subsidence area F1.

Foshan City, Xiaoyong Village (B2), Huadun Village (B11), Yingming Village (B12), as well as those in Shunde District, Foshan City (including Huoshi Street (B3), Yongsheng Village (B4)), Hengjiang Village (B6), the East Village (B9) in Nanhai District, Fengxi Village (B7), Xingguangli Village (B8) in Liwan District, Guangzhou City, and Xingshaxi Village (B10) in Panyu District. Based on high-definition Google Satellite imagery, it was observed that most of the buildings with significant deformation in areas B1, B2, B3, and B4 are low-rise factory buildings and building clusters. Besides, the buildings in areas B4, B8, B9, B10, and B12 are either low-rise factory buildings or buildings that have undergone consecutive demolition or repair during the monitoring period. The buildings in area B5 and B7 are full of low-rise factory buildings.

However, the obvious deformation observed in low-rise buildings within area B6 shows no corresponding ground surface changes. According to further investigation, these anomalies mainly result from phase unwrapping errors in InSAR data, which are caused by abrupt phase discontinuities of surrounding high-rise buildings. Therefore, further attention is required for the hazardous buildings in areas B1 and B2. So, there are still buildings with significant deformation in the study area, but most of the deformations are caused by large-scale activities such as reconstruction, external repair, or demolition through change detection. Some buildings could be influenced by factors such as local water wells, groundwater extraction, and underground engineering, which would require more comprehensive monitoring and field measures.

B. Detailed Health Monitoring of Urban Railways

Fig. 8 shows the cumulative deformation and land cover changes along the subway lines in Foshan. It also presents three enlarged main subsidence areas of Foshan subway lines, which are near Pingshun East road station (F1), Chuangyi station (F2), Huyong station (F3), and Meiqi station (F2). The optical images of three major typical areas acquired in December 2016 and December 2020 are also displayed. It was discovered that subway stations located near the Pingshun East road station (F1) on line 4 exhibited significant large-scale deformations, with a cumulative deformation in the LoS direction reaching −169 mm.

Both the InSAR-based results and that of the optical images show temporal changes of numerous subsidence funnels of varying degrees around the subway lines in Guangzhou [see Fig. 9]. Moreover, it is essential to note that surface alterations of different magnitudes have also been observed in close proximity to several subway lines. As such, these findings demand increased attention and further inspection. Guangzhou's subway routes in operation include 8 separate lines, and another 6 lines have been under construction since 2017. Fig. 9 also shows the deformation rates along the LoS direction and surface changes of six enlarged main subsidence areas of Guangzhou subway

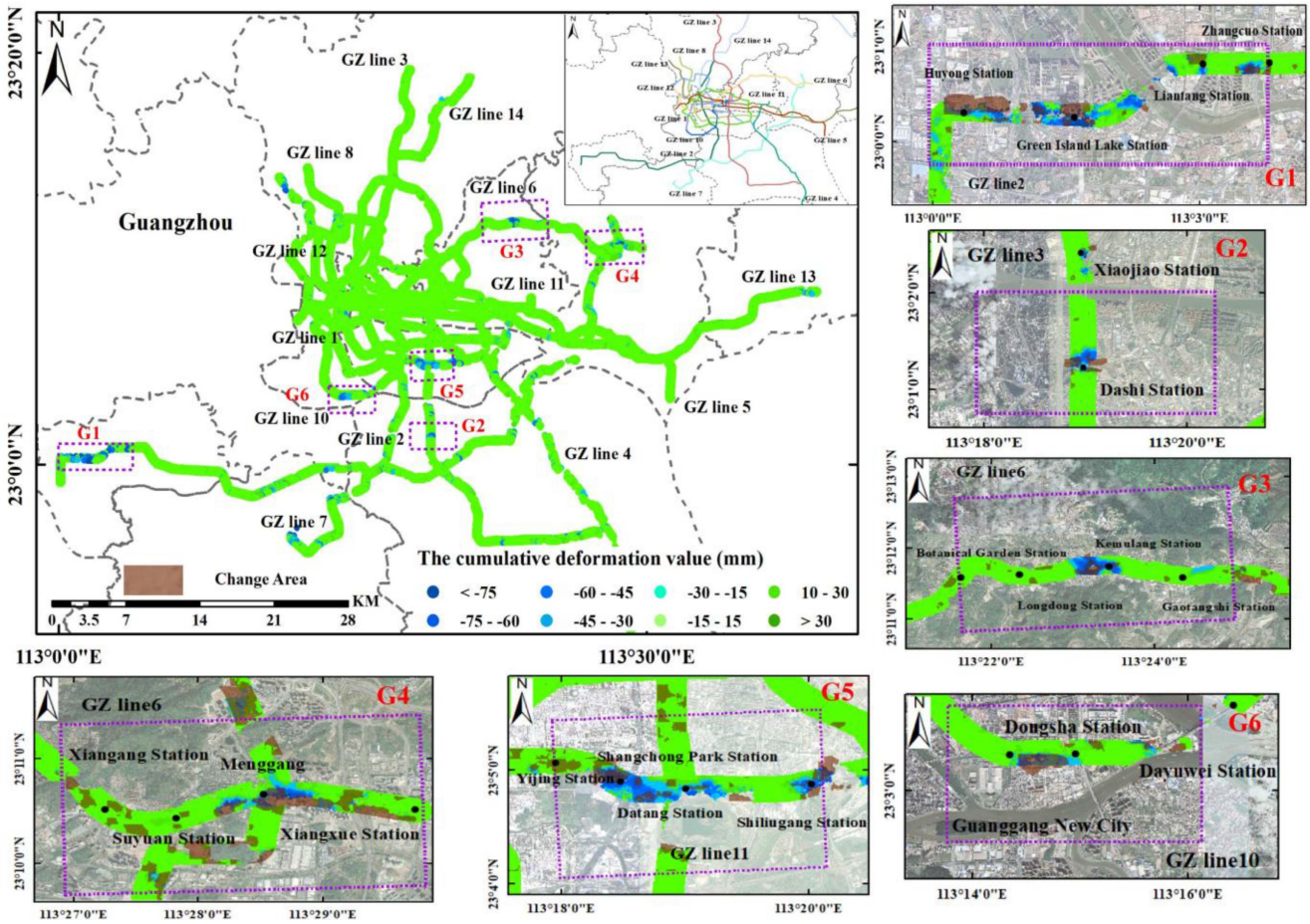

Fig. 9. Annual average subsidence along the LoS direction and urban surface change along the subway line in Guangzhou from March 2017 to April 2020, and six enlarged main subsidence areas of Guangzhou subway lines G1, G2, G3, G4, G5, G6.

lines. These areas are near Green Island Lake station (G1), Dashi station (G2), Kemulang station (G3), Menggang station (G4), Datang station (G5), and Dongsha station (G6), respectively. Land subsidence occurred already at the Green Island lake and Lake Chung Railway stations (G1) of line 2. The largest cumulative deformation along the LoS direction monitored by SAR images is −156 mm. Since the construction of line 2 was completed before the collection of sentinel-1 data, it has been observed that surface construction works took place in the area, which is also shown in Fig. 9.

Therefore, it is likely that the land subsidence was caused by engineering construction activities. Soil disturbance and water loss from foundation pits are common during engineering construction and are the primary causes of subsidence in the surrounding areas. The southern part of the north-south section of line 3 appears relatively stable, but with significant subsidence locations near the Dashi station (G2) in the middle part. Inspections of the optical data reveal significant changes in surface construction, as shown in Fig. 9. The maximum displacement exceeds 8 mm/year.

However, lines 4 and 5 have been operating normally since 2017 and their pathways are generally stable. Although there are still surface changes of varying degrees around them, these changes have had minimal impact on the operation of the subway lines. The overall stability of lines 6 and 8 is relatively good, but there are significant settlement areas at the Kemulang station (G3) and Menggang station (G4) of line 6, and Datang station (G5) of line 8 in Fig. 9. At these places local urban change activities are detectable on the surface. Furthermore, there are multiple subsidence funnels along line 7. Since 2017, Guangzhou has continuously constructed the subway lines 10, 11, 12, 13, and 14. Especially in 2022, line 13 and line 14 (including the knowledge city line) have been put into operation, while other lines are still under construction. As a result, there are varying degrees of subsidence funnels observed along these routes, with significant deformations occurring in the vicinity of the Dongsha station (G6) on line 10, as shown in Fig. 9. This fact is also depicted by the inspection of the optical change map that indicates frequent urban surface change activities in this area.

Table II gives the detailed proportion for InSAR-driven scatterers of buildings and railways at different locations. It has been determined that InSAR-driven building scatterers with the absolute cumulative deformation along the LoS direction of greater than 10 mm constitute 11.57% of the total. Furthermore, 36% of building InSAR driven points cover urban change areas. Besides, it has been determined that InSAR-driven scatterers of railways with the absolute cumulative deformation of greater

TABLE II
INSAR DRIVEN POINTS AT DIFFERENT LOCATIONS

	Absolute annual deformation (<10 mm)	**Absolute annual deformation (>10 mm)**	
All InSAR scatterers of buildings	88.7%	11.53%	
		Covering urban surface change	Covering other places
		36%	64%
	Absolute annual deformation (<10 mm)	Absolute annual deformation (>10 mm)	
All InSAR scatterers of railways	91.25%	9.75%	
		Covering urban surface change	Covering other places
		33.8%	66.2%

than 10 mm constitute 9.75% of the total. Furthermore, 33.38% of these scatterers of railways cover urban change areas. Notably, the absolute cumulative deformation along the LoS direction of InSAR-driven scatterers for all buildings or railways covering the change area is predominantly less than 10 mm. This indicates that larger deformations of a high proportion of urban buildings or railways as detected by InSAR technology are caused by construction works, repair, and demolition.

To validate the accuracy of the experiment, we made a comparison between our results and those of previous monitoring. COSMO-SkyMed images were investigated and showed many local subsidence phenomena, which were caused by the excessive extraction of groundwater [30]. *L*-band synthetic aperture radar (PALSAR) images were used to draw a surface deformation map of the Guangzhou metro network. It was observed that deformation along certain subway sections is significantly influenced by adjacent urban construction activities [31]. We found that the average regional subsidence rate of the newly constructed tunnels exceeds 8 mm per year. Using Landsat-8 imagery, urban expansion in Foshan, Guangdong was investigated for the 2017–2022 period, revealing measurable increases in built-up areas [32], [33]. The outcomes of previous investigations into various local urban infrastructures and urban built-up change activities are highly consistent with our own results, although the specific annual average deformation rate deviates due to different data collection periods and data characteristics.

V. CONCLUSION

To conduct a detailed health monitoring of large-scale urban infrastructure, we have undertaken a detailed study of integrating InSAR and optical techniques. The SBAS-InSAR method and ChangeClip model are utilized for slow deformation monitoring and sharp deformation detection of urban infrastructure. Subsequently, the ICA method is used to gain a more in-depth understanding of the progress of urban slow deformation over time. It is observed that there are numerous irregular slow deformation funnels of different scales in Guangzhou and Foshan. The majority of these deformation events are linked to the process of urbanization. Furthermore, by overlapping the optical sharp deformation detection map generated by the ChangeClip big model with the InSAR-based infrastructure slow deformation map, we conducted a precise identification of the detailed health monitoring of large-scale urban infrastructure. It revealed that the majority of observed deformations of large-scale urban infrastructure in the past two years can be attributed to construction works at these facilities and surrounding objects. Some ground infrastructures, such as high-rise buildings with significant deformation, were found. It is found that surface deformation signals around certain urban areas are more pronounced, thereby realizing the detailed monitoring of urban surface activities.

Due to the relatively low spatial resolution of sentinel-1 SAR data, we face problems in phase shift and signal loss in deformation monitoring of urban areas. In our future work, we will utilize high-resolution SAR imagery to meticulously monitor the slow deformation of infrastructure, with a particular focus on buildings. Additionally, leveraging high-resolution optical imagery, we will establish a sample dataset and develop change detection models to identify significant changes in infrastructure characteristics, such as building heights and rooftops, thereby detecting abrupt deformations. By integrating high-resolution optical imagery with SAR-derived deformation data, we aim to accurately detect significant changes in infrastructure features, eliminate pseudo-hazardous infrastructure, and ultimately enable refined screening of large-scale infrastructure networks, particularly buildings.

ACKNOWLEDGMENT

The authors are grateful to the German Aerospace Centre (DLR) for the supply of the TerraSAR-X data. The authors sincerely appreciate the anonymous reviewers' diligent work and insightful feedback, which significantly contributed to improving the quality of this article.

REFERENCES

[1] F. Qu, Q. Zhang, Z. Lu, C. Zhao, C. Yang, and J. Zhang, "Land subsidence and ground fissures in Xi'an, China 2005–2012 revealed by multi-band InSAR time-series analysis," *Remote Sens. Environ.*, vol. 155, pp. 366–376, 2014.

[2] M. Motagh et al., "Quantifying groundwater exploitation induced subsidence in the Rafsanjan plain, Southeastern Iran, using InSAR time-series and in situ measurements," *Eng. Geol.*, vol. 218, pp. 134–151, 2017.

[3] M. H. Haghighi and M. Motagh, "Ground surface response to continuous compaction of aquifer system in Tehran, Iran: Results from a long-term multi-sensor InSAR analysis," *Remote Sens. Environ.*, vol. 221, pp. 534–550, 2019.
[4] Y. He, G. Xu, H. Kaufmann, J. Wang, H. Ma, and T. Liu, "Integration of InSAR and LiDAR technologies for a detailed urban subsidence and hazard assessment in Shenzhen, China," *Remote Sens.*, vol. 13, no. 12, 2021, Art. no. 2366.
[5] A. Ciampalini et al., "Analysis of building deformation in landslide area using multisensor PSInSAR^{TM} technique," *Int. J. Appl. Earth Observ. Geoinf.*, vol. 33, pp. 166–180, 2014, doi: 10.1016/j.jag.2014.05.011.
[6] Z. Yang et al., "An InSAR-based temporal probability integral method and its application for predicting mining-induced dynamic deformations and assessing progressive damage to surface buildings," *IEEE J. Sel. Top. Appl. Earth Observ. Remote Sens.*, vol. 11, no. 2, pp. 472–484, Feb. 2018, doi: 10.1109/JSTARS.2018.2789341.
[7] P. Ma, Y. Zheng, Z. Zhang, Z. Wu, and C. Yu, "Building risk monitoring and prediction using integrated multi-temporal InSAR and numerical modeling techniques," *Int. J. Appl. Earth Observ. Geoinf.*, vol. 114, 2022, Art. no. 103076, doi: 10.1016/j.jag.2022.103076.
[8] Q. Li, W. Wang, J. Wang, J. Zhang, and D. Geng, "Exploring the relationship between InSAR coseismic deformation and earthquake-damaged buildings," *Remote Sens. Environ.*, vol. 262, 2021, Art. no. 112508, doi: 10.1016/j.rse.2021.112508.
[9] C.-W. Lee, Z. Lu, and H.-S. Jung, "Simulation of time-series surface deformation to validate a multi-interferogram InSAR processing technique," *Int. J. Remote Sens.*, vol. 33, no. 22, pp. 7075–7087, 2012.
[10] M. Zhu et al., "Detection of building and infrastructure instabilities by automatic spatiotemporal analysis of satellite SAR interferometry measurements," *Remote Sens.*, vol. 10, no. 11, 2018, Art. no. 1816.
[11] A. D. Boloorani, M. Darvishi, Q. Weng, and X. Liu, "Post-war urban damage mapping using InSAR: The case of Mosul City in Iraq," *ISPRS Int. J. Geo-Inf.*, vol. 10, no. 3, 2021, Art. no. 140.
[12] V. Macchiarulo, P. Milillo, C. Blenkinsopp, and G. Giardina, "Monitoring deformations of infrastructure networks: A fully automated GIS integration and analysis of InSAR time-series," *Struct. Health Monit.*, vol. 21, no. 4, pp. 1849–1878, 2022.
[13] Z. Liu, G. Mei, Y. Sun, and N. Xu, "Investigating mining-induced surface subsidence and potential damages based on SBAS-InSAR monitoring and GIS techniques: A case study," *Environ. Earth Sci.*, vol. 80, no. 24, 2021, Art. no. 817, doi: 10.1007/s12665-021-09726-z.
[14] P. S. J. Minderhoud, L. Coumou, L. E. Erban, H. Middelkoop, E. Stouthamer, and E. A. Addink, "The relation between land use and subsidence in the Vietnamese Mekong delta," *Sci. Total Environ.*, vol. 634, pp. 715–726, 2018, doi: 10.1016/j.scitotenv.2018.03.372.
[15] L. Guo et al., "Mechanism of land subsidence mutation in Beijing plain under the background of urban expansion," *Remote Sens.*, vol. 13, no. 16, 2021, Art. no. 3086, doi: 10.3390/rs13163086.
[16] J. Zhang, C. Ke, X. Shen, J. Lin, and R. Wang, "Monitoring land subsidence along the subways in Shanghai on the basis of time-series InSAR," *Remote Sens.*, vol. 15, no. 4, 2023, Art. no. 908, doi: 10.3390/rs15040908.
[17] J. Cai, L. Zhang, J. Dong, J. Guo, Y. Wang, and M. Liao, "Automatic identification of active landslides over wide areas from time-series InSAR measurements using faster RCNN," *Int. J. Appl. Earth Observ. Geoinf.*, vol. 124, 2023, Art. no. 103516, doi: 10.1016/j.jag.2023.103516.
[18] A. Hyvärinen and E. Oja, "Independent component analysis: Algorithms and applications," *Neural Netw.*, vol. 13, no. 4-5, pp. 411–430, 2000.
[19] A. Hyvarinen, "Fast and robust fixed-point algorithms for independent component analysis," *IEEE Trans. Neural Netw.*, vol. 10, no. 3, pp. 626–634, May 1999.
[20] J. Li, W. He, Z. Li, Y. Guo, and H. Zhang, "Overcoming the uncertainty challenges in detecting building changes from remote sensing images," *ISPRS J. Photogramm.Remote Sens.*, vol. 220, pp. 1–17, 2025, doi: 10.1016/j.isprsjprs.2024.11.017.
[21] X. Zhang, H. Chen, Y. Zhao, M. He, and X. Han, "Change detection of buildings in remote sensing images using a spatially and contextually aware Siamese network," *Expert Syst. Appl.*, vol. 276, 2025, Art. no. 127110, doi: 10.1016/j.eswa.2025.127110.
[22] Y. He et al., "Detailed hazard identification of urban subsidence in Guangzhou and Foshan by combining InSAR and optical imagery," *Int. J. Appl. Earth Observ. Geoinf.*, vol. 135, 2024, Art. no. 104291, doi: 10.1016/j.jag.2024.104291.
[23] P. Berardino, G. Fornaro, R. Lanari, and E. Sansosti, "A new algorithm for surface deformation monitoring based on small baseline differential SAR interferograms," *IEEE Trans. Geosci. Remote Sens.*, vol. 40, no. 11, pp. 2375–2383, Nov. 2002, doi: 10.1109/TGRS.2002.803792.
[24] C. Zhang, Z. Li, C. Yu, C. Song, R. Xiao, and J. Peng, "Landslide detection of the Jinsha River Region using GACOS assisted InSAR stacking," *Geomatics Inf. Sci. Wuhan Univ.*, vol. 46, no. 11, pp. 1649–1657, 2021.
[25] M. E. Gaddes, A. Hooper, M. Bagnardi, H. Inman, and F. Albino, "Blind signal separation methods for InSAR: The potential to automatically detect and monitor signals of volcanic deformation," *J. Geophys. Res., Solid Earth*, vol. 123, no. 11, pp. 10–226, 2018.
[26] A. Kirillov, E. Mintun, N. Ravi, H. Mao, C. Rolland, and L. Gustafson, "Segment anything," in *Proc. IEEE/CVF Int. Conf. Comput. Vis.*, 2023, pp. 4015–4026.
[27] M. A. Mazurowski, H. Dong, H. Gu, J. Yang, N. Konz, and Y. Zhang, "Segment anything model for medical image analysis: An experimental study," *Med. Image Anal.*, vol. 89, 2023, Art. no. 102918, doi: 10.1016/j.media.2023.102918.
[28] S. Dong, L. Wang, B. Du, and X. Meng, "ChangeCLIP: Remote sensing change detection with multimodal vision-language representation learning," *ISPRS J. Photogramm. Remote Sens.*, vol. 208, pp. 53–69, 2024, doi: 10.1016/j.isprsjprs.2024.01.004.
[29] F. Chen, H. Lin, Y. Zhang, and Z. Lu, "Ground subsidence geo-hazards induced by rapid urbanization: Implications from InSAR observation and geological analysis," *Natural Hazards Earth Syst. Sci.*, vol. 12, no. 4, pp. 935–942, 2012.
[30] A. H.-M. Ng et al., "InSAR reveals land deformation at Guangzhou and Foshan, China between 2011 and 2017 with COSMO-SkyMed data," *Remote Sens.*, vol. 10, no. 6, 2018.
[31] H. Wang et al., "Deriving spatio-temporal development of ground subsidence due to subway construction and operation in delta regions with PS-InSAR data: A case study in Guangzhou, China," *Remote Sens.*, vol. 9, no. 10, 2017, Art. no. 1004.
[32] Y. Lei, H. Cao, X. Zhou, J. Mills, and W. Xiao, "Impact of land use/land cover changes on urban flooding: A case study of the Greater Bay Area, China," *IEEE J. Sel. Top. Appl. Earth Observ. Remote Sens.*, vol. 17, pp. 13261–13275, 2024.
[33] X. QIN et al., "Urban built-up area extraction and risk analysis of Guangzhou City by integrating InSAR and optical remote sensing," *Geomatics Inf. Sci. Wuhan Univ.*, vol. 50, no. 8, pp. 1583–1598, 2025.

Yufang He received the M.S. degree in geodesy and survey engineering from Chang'an University, Xi'an, China, in 2019, and the Ph.D. degree in aerospace science and technology from Harbin Institute of Technology, Shenzhen, China, in 2024.

Her research interests include machine learning and its applications in monitoring of surface subsidence based on InSAR technology.

Lifeng Niu received the M.S. degree in cartography and geographic information system from Lanzhou Jiaotong University, Lanzhou, China, in 2020. She is currently working toward the Ph.D. degree in machine with Harbin Institute of Technology, Shenzhen, China.

Her research interests include machine learning and its applications in nearshore ecological environment.

Guangzong Zhang received the M.S. degree in geography from Ludong University, Yantai, China, in 2020. He is currently working toward the Ph.D. degree in machine with Harbin Institute of Technology, Shenzhen, China.

His research interests include deep learning and its applications on ocean color of remote sensing and harmful algae image classification.

Jiaye Li received the Ph.D. degree in hydraulics and river dynamics from Tsinghua University, Beijing, China, in 2018.

His research focuses on digital river basin technologies and smart water resources systems. He also explores AI-enhanced remote sensing applications for hydrological monitoring, disaster prediction, and watershed governance.

Tong Liu received the Ph.D. degree in aerospace science and technology from Harbin Institute of Technology, Shenzhen, China, in 2023.

His research interests include ionospheric observation, modeling and prediction, as well as the impact of space weather on GNSS and corresponding mitigation strategies.

Jian Liu received the Ph.D. degree in aerospace science and technology from Harbin Institute of Technology, Shenzhen, China, in 2023.

His research interests include GNSS signal processing, integrated navigation, and robust estimation.

Bo Chen (Member, IEEE) received the B.E. degree in aerial photogrammetry and the Ph.D. degree in photogrammetric engineering and remote sensing from Information Engineering University, Zhengzhou, China, in 2002 and 2008, respectively.

Since 2020, he has been a Full Professor with the Institute of Space Science and Applied Technology, Harbin Institute of Technology (Shenzhen), Shenzhen, China. His research interests include satellite-on-orbit computing, geospatial Big Data, and spatial information engineering.